

Spatiotemporal dynamics of coupled-transverse-mode oscillations in unidirectional photorefractive ring resonators

B. M. Jost

Department of Electrical and Computer Engineering, University of Wisconsin–Madison, Madison, Wisconsin 53706

B. E. A. Saleh

Department of Electrical and Computer Engineering, University of Wisconsin–Madison, Madison, Wisconsin 53706 and Department of Electrical, Computer, and Systems Engineering, Boston University, Boston, Massachusetts 02215

(Received 31 May 1994)

We examine the spatiotemporal dynamics of the optical field that arises from two-wave mixing in a multiple-transverse-mode unidirectional photorefractive ring resonator. Using the passive resonator's transverse modes as a basis, we derive a set of differential equations that describes the mode dynamics when both pump-mode and mode-mode gratings are formed. In the absence of intermodal gratings, this set reduces to the Hopf bifurcation equations for nonlinear mode interactions. We have performed two and three transverse-mode experiments using a photorefractive ring resonator with an Fe:KNbO₃ crystal. Numerically simulated coupled-mode dynamics are shown to have good correspondence with the experimental data.

PACS number(s): 42.50.Ne, 42.65.Hw, 05.45.+b

I. INTRODUCTION

There is much current interest in the spatiotemporal dynamics of optical phenomena, both to develop an understanding of them and to determine their significance in applications. In particular, the spatiotemporal dynamics of optical oscillations in photorefractive [1–11] and laser [12–16] resonators have recently received considerable attention. The analyses of these systems have demonstrated many interesting phenomena, including periodic and chaotic mode alternation, optical defect dynamics, and general spatiotemporal complexity.

Oscillations develop in a unidirectional photorefractive ring resonator (UPRR) when light from a laser is used to pump a photorefractive crystal within an optical cavity [17]. The resonator beam interferes with the pump beam inside the crystal and, when the crystal is properly oriented, the resulting interference pattern creates index of refraction variations that refract pump light into the resonator. Consequently, the resonator field grows until saturation effects balance the amplification. As in the laser, the spatial pattern of the oscillations depends on the geometry of the optical cavity and the characteristics of the active medium.

Experiments by Arecchi *et al.* [5–7] and Hennequin *et al.* [8] have demonstrated many of the interesting aspects of multiple-transverse-mode oscillations in a UPRR. For example, Arecchi *et al.* have obtained periodic and chaotic mode alternation and spatiotemporally chaotic optical vortex distributions. Spatiotemporal chaos was shown to occur in the large Fresnel number limit [5] and scaling exponents for various quantities related to the observed optical defects were calculated from the experimental data [6]. Hennequin *et al.* [8] have demonstrated that periodic two-mode mixing occurs in UPRRs, both with frequency degenerate families and

with nondegenerate families of modes. These and similar results reported in the present work indicate the extent to which mode coupling influences UPRR dynamics.

A basic theoretical description of multiple-mode UPRR dynamics was first given by Anderson and Saxena [2], who showed that there was stronger mode competition between modes with similar transverse distributions than those with dissimilar distributions. Arecchi *et al.* [7] have shown that periodic and chaotic alternation in UPRRs with circular apertures can arise from an imperfect O(2) symmetry. A multiple-mode analysis that neglects intermodal gratings but retains mode coupling through a projection of the modes onto the refractive index grating has been developed by D'Alessandro [9]. Numerical evaluations from this analysis were able to demonstrate some of the spatiotemporal effects observed in the experiments by Arecchi *et al.* [5,6]; however, the general spatiotemporal complexity observed in the experiments could only be duplicated with parameter values that were inconsistent with the assumptions of the analysis. Recently, Jost and Saleh [10] have shown that the nonlinear spatiotemporal oscillations in a UPRR are governed by a complex Ginzburg-Landau equation, thus the UPRR may be a useful system for the general study of the spatiotemporal dynamics of complex fields.

In this paper, we examine the effects of intermodal gratings on the spatiotemporal dynamics of multiple-transverse-mode UPRR oscillations. In Sec. II we generalize the work of Anderson and Saxena [2] and D'Alessandro [9] to include intermodal gratings in the coupled-mode equations that govern the optical field and refractive index gratings amplitudes. Additional distinctions from previous analyses are that we include the effects of the photorefractive time constant's total intensity dependence, and we retain the time constant's and the coupling constant's complex forms. These two constants

are complex when there is either an applied dc field across the photorefractive crystal or when photovoltaic effects are substantial. In Sec. III we present examples of the field and grating dynamics obtained from the numerical integration of the coupled equations. Section IV describes UPRR experiments performed using an Fe:KNbO₃ (iron-doped potassium niobate) crystal. This section provides detailed reports on the transverse-mode dynamics in a UPRR without an applied electric field across the crystal. The spatiotemporal data from the experiments are shown to be in general agreement with the theoretical description of Sec. III. We summarize and discuss our results in Sec. V.

II. COUPLED-MODE EQUATIONS

We consider the unidirectional UPRR configuration shown in Fig. 1. The resonator contains a photorefractive crystal illuminated with an undepleted uniform pump beam described by its electric field

$$E_p(\mathbf{r}, t) = \hat{\mathbf{e}}_p E_p \exp[i(\mathbf{k}_p \cdot \mathbf{r} - \omega_p t)] + \text{c.c.}, \quad (2.1)$$

where $\hat{\mathbf{e}}_p$ is the pump polarization vector, E_p is the complex pump field amplitude, and \mathbf{k}_p and ω_p are the pump beam wave vector and frequency, respectively. We have chosen a spatially uniform pump to simplify our analysis; however, a nonuniform pump is expected to affect the spatiotemporal dynamics [10].

The active resonator field is assumed to comprise a complete set of passive cavity modes. Modal decomposition has been used in numerous theoretical resonator analyses [2, 4, 7–9, 11, 12, 14] and has shown good correspondence with experimental results. We write the modes as general complex amplitude spatial functions $\hat{\mathbf{e}}_l W_l(\mathbf{r}) \exp(i\mathbf{k}_l \cdot \mathbf{r})$ where $W_l(\mathbf{r})$ is the slowly varying complex spatial amplitude of the l th passive cavity mode, \mathbf{k}_l is its corresponding wave vector, and $\hat{\mathbf{e}}_l$ is its polarization vector. These functions are chosen to have unity maximum magnitude; that is, they are normalized to have $\max |W_l(\mathbf{r})| = 1$. Also, they are assumed to satisfy the normalization conditions

$$\int_{L_C} \exp(i\mathbf{k}_l \cdot \mathbf{r}) \exp(-i\mathbf{k}_k \cdot \mathbf{r}) dl = L_l \delta_{lk} \quad (2.2a)$$

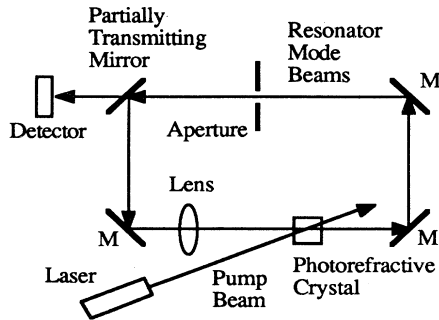


FIG. 1. The experimental configuration for the unidirectional photorefractive ring resonator.

and

$$\int_{S_C} W_l(\mathbf{r}) W_k^*(\mathbf{r}) dS = S_l \delta_{lk}, \quad (2.2b)$$

where L_C and S_C are the cavity length and cross section, respectively, and L_l and S_l are the l th cavity mode's length and cross-section normalization constants, respectively.

We consider the uniform (mean) field limit [2, 7, 9, 10, 12, 15, 17], where the cavity gain and losses are sufficiently small that slowly varying longitudinal variations of the resonator modes can be neglected. Hence the active resonator field can be written

$$E_R(\mathbf{r}, t) = \sum_l \{ \hat{\mathbf{e}}_l V_l(t) W_l(\mathbf{r}) \exp[i(\mathbf{k}_l \cdot \mathbf{r} - \omega_p t)] + \text{c.c.} \}, \quad (2.3)$$

where $V_l(t)$ is a slowly varying temporal envelope, and each l corresponds to a unique set of integers (m_l, n_l, q_l) with m_l, n_l denoting the transverse-mode structure and q_l denoting the longitudinal mode. In addition, $k_l = |\mathbf{k}_l| = \Omega_l \sqrt{\mu_0 \epsilon}$ where k_l and Ω_l are, respectively, the wave number and oscillation frequency of the l th passive cavity mode with $\Omega_l \approx \omega_p$; and μ_0 and ϵ are the linear permeability and permittivity of the medium. We assume that the resonator beam travels along the z axis; the pump and resonator beams are linearly polarized perpendicular to the photorefractive material's crystal axis and they are propagating at small angles to one another; and that the active mode frequencies are nearly equal to the pump frequency with any differences between them small enough to be included in the slowly varying complex amplitudes of the resonator beam.

An optical intensity pattern is formed within the crystal by the interference between the pump and resonator beams,

$$I(\mathbf{r}, t) = \frac{1}{2} [E_p(\mathbf{r}, t) + E_R(\mathbf{r}, t)]^2 = I_0(t) + I_1(\mathbf{r}, t), \quad (2.4)$$

where

$$I_0(t) = |E_p|^2 + \sum_l |V_l(t)|^2 \quad (2.5)$$

and

$$I_1(\mathbf{r}, t) = \sum_n [E_p W_n(\mathbf{r}) V_n^*(t) \exp(i\mathbf{K}_n \cdot \mathbf{r}) + \text{c.c.}] + \sum_n \sum_{l \neq n} [W_l(\mathbf{r}) W_n^*(\mathbf{r}) V_l(t) V_n^*(t) \times \exp(i\mathbf{K}_{ln} \cdot \mathbf{r}) + \text{c.c.}], \quad (2.6)$$

with $\mathbf{K}_n = \mathbf{k}_p - \mathbf{k}_n$, $\mathbf{K}_{ln} = \mathbf{k}_l - \mathbf{k}_n$, and all beams are assumed parallel polarized. Also, we have neglected terms with a $2\omega_p$ time dependence because they are not expected to be supported by the resonator [2].

To make the analysis tractable, we have assumed that the spatial intensity maxima of the modes overlap in the same location and we have used the maximum value of

the mode amplitude $|W_l|=1$ in place of the spatially varying amplitude $|W_l(\mathbf{r})|$ in the expression for $I_0(t)$. The latter simplification is reasonable because $I_0(t)$ determines the saturation value of each mode's amplitude. Since each mode has a spatial intensity that is fixed as a function of location relative to any other point on its wave front, the saturation of one point on the wave front within the amplifying medium—that with the highest intensity—will determine the saturated intensity of the entire modal wave front. The former approximation on the mode overlap location may alter the particular mode amplitudes relative to the case in which the full spatial variations are taken into account; however, we expect the general nature of the results to remain unchanged.

The refractive index change Δn is related to the modulated intensity I_1 through the differential equation [17,18]

$$\left[\frac{\partial}{\partial t} + \frac{1}{\tau(t)} \right] \Delta n(\mathbf{r}, t) = i \frac{\gamma n_s^3 r_{\text{eff}}}{2\tau_c I_P} I_1(\mathbf{r}, t), \quad (2.7)$$

where

$$\tau(t) = \frac{\tau_I(t)}{(E_q + E_d)^2 + E_0^2} [(E_\mu + E_d)(E_q + E_d) + E_0^2 + iE_0(E_\mu - E_q)] \quad (2.8)$$

is the intensity-dependent complex time constant,

$$\gamma = \frac{E_q}{(E_q + E_d)^2 + E_0^2} \{ E_d(E_q + E_d) - E_0(E_v - E_0) + i[E_q(E_v - E_0) + E_d E_v] \} \quad (2.9)$$

is the complex coupling constant, and $\tau_c = \tau I_0 / I_P$ is the complex photorefractive time constant. This equation has been obtained from a reduced set [10,17] of the Kukhtarev equations [19]. In Eqs. (2.8) and (2.9), E_0 is the total external dc electric field, E_v is the photovoltaic field, $E_d \sim K_T$ is the diffusion field, $E_q \sim 1/K_T$ is the limiting space-charge field, $E_\mu \sim 1/K_T$ is the drift field, and $\tau_I \sim 1/I_0$ is the photoproduction time. Note that K_T is equivalent to K_n or K_{ln} depending on the context and that $\tau(t)$ and γ are mode dependent even though we do not explicitly indicate it here. Also, we have defined the complex photorefractive time constant $\tau_c = \tau(t)I_0(t)/I_P$ since $\tau(t) \sim 1/I_0(t)$.

We desire an explicit solution for the refractive index change in Eq. (2.7) and, under certain conditions, a relatively simple form is possible. First, for $d\tau/dt \ll 1$, the solution to Eq. (2.7) is space-time separable [17,18]. Second, recent steady-state studies indicate that when the external field is small ($E_0 \ll 10 \text{ kV cm}^{-1}$) and there is a relatively large probe-to-pump ratio [approximately $1 \gg (I_0 - I_P)/I_P \gg 0.01$], the refractive index distribution within the photorefractive crystal is approximately proportional to the optical intensity distribution [20]. Note that when these conditions are violated, the refractive index distribution becomes spatially distorted (relative to the intensity) and the index may contain longitudinal variations that invalidate the uniform field limit. We

assume that the external field and the intensity ratio satisfy the two conditions for our analysis. As a consequence, the refractive index variation can be expanded in the same subset of modes as the field distribution. Thus we write the refractive index in the form of the intensity distribution

$$\Delta n(\mathbf{r}, t) = \sum_m \{ G_m(t) W_m(\mathbf{r}) \exp[i(\mathbf{K}_m \cdot \mathbf{r})] + \text{c.c.} \} + \sum_{m \neq p} \{ G_{pm}(t) W_p(\mathbf{r}) W_m^*(\mathbf{r}) \times \exp[i(\mathbf{K}_{pm} \cdot \mathbf{r})] + \text{c.c.} \}, \quad (2.10)$$

where $G_m(t)W_m(\mathbf{r})$ is the pump-mode coupling contribution, and $G_{pm}(t)W_p(\mathbf{r})W_m^*(\mathbf{r})$ is the mode-mode coupling contribution to the refractive index change's slowly varying spatiotemporal amplitude.

Substituting Eqs. (2.6) and (2.10) into Eq. (2.7), and matching wave numbers so that $K_l = K_n$ for $l = n$ and $K_{mn} = K_{pl}$ for $l = n \neq m = p$, we obtain the equations for the n th and m th slowly varying index grating components

$$\frac{dG_n(t)}{dt} = D_n V_n^*(t) + F_n \left[|E_P|^2 + \sum_l |V_l|^2 \right] G_n(t), \quad (2.11)$$

where

$$D_n = iE_P \Gamma_n, \quad (2.12a)$$

$$F_n = -\frac{1}{I_P \tau_{cn}}, \quad (2.12b)$$

with $\Gamma_n = \gamma n_s^2 r_{\text{eff}} / 2I_P \tau_{cn}$, n_s the static refractive index, and r_{eff} the effective electro-optic coefficient of the photorefractive material. For $m \neq n$,

$$\frac{dG_{mn}(t)}{dt} = D_{mn} V_n^*(t) V_m(t) + F_{mn} \left[|E_P|^2 + \sum_l |V_l|^2 \right] G_{mn}(t), \quad (2.13)$$

where

$$D_{mn} = iI_P \Gamma_{mn}, \quad (2.14a)$$

$$F_{mn} = -\frac{1}{I_P \tau_{cmn}}, \quad (2.14b)$$

with $\Gamma_{mn} = \gamma_{mn} n_s^3 r_{\text{eff}} / 2I_P \tau_{cmn}$. Also, we have now explicitly shown the mode dependences of all the relevant constants. In our model, modes which have significantly smaller values of Γ_n and Γ_{mn} than the others are simply expected not to oscillate and can be excluded from consideration.

In general, significant intermodal gratings do not require \mathbf{K}_n to be parallel to \mathbf{K}_{mn} , since the change in the refractive index depends on the orientation of the grating vector with respect to the crystal directions having a large electro-optic coefficient. The crystal may not be aligned for maximum index change in conjunction with \mathbf{K}_n . Nor does it require $K_n = K_{mn}$, since the index

change can increase with decreasing angle between beams when there is an applied electric field [21] or when photo-voltaic effects are significant. This is important because $K_{mn} \ll K_n$ due to the angular dependences of the wave vectors and because the index change typically decreases with decreasing grating wave number in the absence of bulk electric field effects [21].

For simplicity, we consider a photorefractive medium that has a single axis having a strong electro-optic coefficient and that it is aligned with the crystal axis. In the pump-mode interaction, we assume that energy is unidirectionally given up by the pump to the mode beam, i.e., in the direction of the grating vector (taken to be approximately aligned with the crystal axis). In the mode-mode interaction, we assume that there is a mutual energy exchange [22] between the modes with $\Gamma_{mn} \approx \Gamma_m$. This bidirectionality of the energy exchange between modes permits coupled-mode oscillations when there are intermodal refractive index gratings.

We consider a cavity with longitudinal losses due to cavity imperfections that are described by the loss coefficient α_L . Hence the resonator field must satisfy the wave equation [10,17]

$$\begin{aligned} \nabla^2 \mathbf{E}_R - \frac{\alpha_L}{2\pi} \sqrt{\mu_0 \epsilon} \frac{\partial \mathbf{E}_R}{\partial t} - \mu_0 \epsilon \frac{\partial^2 \mathbf{E}_R}{\partial t^2} \\ = -\frac{1}{\epsilon} \nabla(\nabla \cdot \mathbf{P}_{NL}) + \mu_0 \frac{\partial^2 \mathbf{P}_{NL}}{\partial t^2}, \end{aligned} \quad (2.15)$$

where

$$\mathbf{P}_{NL}(\mathbf{r}, t) = 2\epsilon_0[\mathbf{E}_P(\mathbf{r}, t) + \mathbf{E}_R(\mathbf{r}, t)]\Delta n(\mathbf{r}, t) \quad (2.16)$$

is the nonlinear polarization of the cavity medium. We see that \mathbf{P}_{NL} comprises modal amplitude spatial functions through \mathbf{E}_R . Thus a projection procedure can be used to simplify Eq. (2.15).

Substituting Eqs. (2.3) and (2.16) into Eq. (2.15), using the slowly varying envelope and mean field approximations, multiplying by \mathbf{E}_R^* , integrating over the cavity volume, and matching phases on both sides of the resulting equation, we obtain the cavity field equation

$$\frac{dV_n(t)}{dt} = A_n V_n(t) + B_n G_n^*(t) + \sum_{m \neq n} C_{mn} V_m(t) G_{mn}^*(t), \quad (2.17)$$

with

$$A_n = -\frac{c}{4\pi}(\alpha_{Ln} + i\alpha_{Tn}) - i(\Omega_n - \omega_p), \quad (2.18a)$$

where the mode-dependent longitudinal and transverse loss coefficients α_{Ln} and α_{Tn} , respectively, have been introduced; and α_{Tn} has been obtained from the projection procedure. The other coefficients are defined by

$$B_n = iE_P \frac{\omega_p}{\epsilon_\tau} \rho_n, \quad (2.18b)$$

$$\begin{aligned} \rho_n = \frac{1}{S_n L_n} \int_{s_c} \int_{l_c} W_m(\mathbf{r}) W_n^*(\mathbf{r}) \\ \times \exp[i(\mathbf{k}_m - \mathbf{k}_n) \cdot \mathbf{r}] dS dl, \end{aligned} \quad (2.18c)$$

where $\rho_n \approx l_c/L_C$ is a filling factor, and

$$C_{mn} = i \frac{\omega_n}{\epsilon_r S_n} \int_{s_c} |W_m(\mathbf{r})|^2 |W_n(\mathbf{r})|^2 dS. \quad (2.18d)$$

We note that the coupling coefficient Eq. (2.18d) is of the same form as the two-mode steady-state coupling coefficient calculated in Ref. [2].

A suitable normalization for the study of Eqs. (2.11), (2.13), and (2.17) is obtained by letting $v_n = V_n/E_P$, $g_n = G_n/I_P$, and $g_{mn} = G_{mn}/I_P$ where $I_P = |E_P|^2$. Consequently, these equations become

$$\frac{dv_n(t)}{dt} = a_n v_n(t) + b_n g_n^*(t) + \sum_{m \neq n} c_{mn} v_m(t) g_{mn}^*(t), \quad (2.19)$$

$$\frac{dg_n(t)}{dt} = d_n v_n^*(t) + f_n \left[1 + \sum_l |v_l(t)|^2 \right] g_n(t), \quad (2.20)$$

and for $m \neq n$

$$\begin{aligned} \frac{d - g_{mn}(t)}{dt} = d_{mn} v_m(t) v_n^*(t) \\ + f_{mn} \left[1 + \sum_l |v_l(t)|^2 \right] g_{mn}(t), \end{aligned} \quad (2.21)$$

where

$$a_n = -\frac{c}{4\pi}(\alpha_{Ln} + i\alpha_{Tn}) - i(\Omega_n - \omega_p), \quad (2.22a)$$

$$b_n = iI_P \frac{\omega_p}{\epsilon_\tau} \rho_n, \quad (2.22b)$$

$$c_{mn} = i \frac{\omega_p I_P}{\epsilon_r S_n} \int_{s_c} |W_m(\mathbf{r})|^2 |W_n(\mathbf{r})|^2 dS, \quad (2.22c)$$

$$d_n = i\Gamma_n, \quad (2.22d)$$

$$f_n = -\frac{1}{\tau_{cn}}, \quad (2.22e)$$

$$d_{mn} = iI_P \Gamma_{mn}, \quad (2.22f)$$

and

$$f_{mn} = -\frac{1}{\tau_{cmn}}. \quad (2.22g)$$

For N transverse optical modes generating $N + (N, 2)$ (binomial coefficient) gratings, Eqs. (2.19)–(2.21) define the $N^2 + N$ complex, coupled, nonlinear ordinary differential equations necessary for the description of coupled-mode UPRR dynamics. This is the main result of our analysis.

In the absence of intermodal gratings we can neglect Eq. (2.21) and when $|\tau_\alpha| \ll |\tau_c|$ we can adiabatically eliminate Eq. (2.19) [10,17] so that Eqs. (2.19)–(2.21) reduce to

$$\frac{dv_n(t)}{dt} = \left[f_n^* - \frac{b_n}{a_n} d_n^* \right] v_n(t) + f_n^* v_n(t) \sum_l |v_l(t)|^2. \quad (2.23)$$

This is the normal form equation for Hopf bifurcations in nonlinear mode interactions, which has been extensively examined [23].

When small geometrical asymmetries exist in an otherwise circularly symmetric cavity, a perturbation term equal to $\sum_{m \neq n} \varepsilon_{mn} v_m(t)$, where ε_{mn} is a small mode-dependent complex constant, is added to the right-hand side of Eq. (2.23) [7,23]. In this case, we obtain the broken symmetry Hopf bifurcation equation. Although the set of coupled-mode equations in general does not reduce to the broken symmetry Hopf equation, it is likely that intermodal gratings have an effect that is similar to geometrical asymmetries.

With the full coupled set [Eqs. (2.19)–(2.21)], one can still adiabatically eliminate Eq. (2.19) [9,10,17]. This reduces the phase space variables to $g_n(t)$ and $g_{mn}(t)$. However, because of the coupling term on the right-hand side of Eq. (2.19), adiabatic elimination does not lead to a significant simplification of the governing equations even if the mode coupling is weak. Consequently, further examinations consider the full set of coupled-mode equations.

III. NUMERICAL EVALUATION

We have evaluated the coupled-mode equations [Eqs. (2.19)–(2.21)] by numerically integrating them with the stiff differential equation solver of the advanced continuous simulation language [24]. In our simulations, we have calculated the mode coupling coefficients by assuming the occurrence of a few low-order Hermite-Gaussian modes within the resonator (this choice of modes is not critical to the outcome of the simulations). In particular, we consider modes limited in one dimension to the fundamental mode of the resonator. We also assume that only one family of longitudinal modes can exist in the resonator. Consequently, the modes can be written $W_n(\mathbf{r}) = \omega_n(x, y) \exp[i\phi_n(\mathbf{r})]$ where ω_n and ϕ_n are real and $\omega_n(x, y) = H_{0n}(x, y) \exp[-(x^2 + y^2)/W_0]$ with W_0 the beam waist. H_{mn} is the label for the Hermite-Gaussian function with m and n integers that denote the spatial structure in the x and y directions, respectively.

Table I provides examples of the coupling integrals

$$I_{mn} = \frac{1}{S_n} \int_{s_c} |H_{0m}(x, y)|^2 |H_{0n}(x, y)|^2 \times \exp[-2(x^2 + y^2)/W_0] dS \quad (3.1)$$

that appear in Eq. (2.22c). These coefficients were calculated assuming that the Hermite-Gaussian modes are aligned along the resonator's axis and normalized to unity maximum value. In the absence of mode coupling, $c_{mn} \sim I_{mn} = 0$ and one mode always dominates in our simulations of Eqs. (2.19)–(2.21). By including the effects of intermodal gratings in our model, we have found that multiple modes can coexist in the resonator

TABLE I. Values of the Hermite-Gaussian mode coupling integrals, I_{mn} , which are defined by Eq. (3.1).

$n \backslash m$	0	1	2	3
0	x	0.2500	0.1875	0.1563
1	0.3398	x	0.2973	0.2336
2	0.2855	0.3331	x	0.3034
3	0.2559	0.2815	0.3263	x

even if they have relatively large differences in their loss coefficients.

To determine the physical significance of our results, we write $v_n(t) = a_n(t) \exp[i\theta_n(t)]$ where a_n and θ_n are real. The total normalized intensity at the output of the resonator can then be written

$$I(\mathbf{r}, t) = \left| \sum_n \omega_n(x, y) \exp[i\phi_n(\mathbf{r})] a_n(t) \exp[i\theta_n(t)] \right|^2 \\ = \sum_n \omega_n^2(x, y) a_n^2(t) \\ + \sum_{n, m \neq n} \omega_n(x, y) \omega_m(x, y) a_n(t) a_m(t) \\ \times \cos[\Delta\theta_{nm}(t) + \Delta\phi_{nm}(\mathbf{r})], \quad (3.2)$$

where the intermodal phase differences are $\Delta\theta_{mn}(t) = \theta_n(t) - \theta_m(t)$ and $\Delta\phi_{nm}(\mathbf{r}) = \phi_n(\mathbf{r}) - \phi_m(\mathbf{r})$. The final term in Eq. (3.2) is an interference term whose contribution to the total intensity depends on both the amplitudes of the modes and their phase differences as a function of time and space. For Hermite-Gaussian modes in a cavity with a large Rayleigh range $z_0 \gg L_C$, $\Delta\phi_{nm}$ is negligible; hence we will neglect it in our analyses. In general, $|\cos[\Delta\theta_{nm}(t)]|$ can be expected to vary from 0 to 1.

A. Two modes

In this section, we consider a UPRR that is limited to having only the H_{00} and H_{01} Hermite-Gaussian modes in oscillation. We present an example from our simulations and we summarize some of the general trends we have found.

In our model, we have found that two-mode intensity oscillations of the form shown in Fig. 2 may occur. Figure 2(a), which shows the variations in the peak intensities of the two modes, demonstrates the effects of two-mode coupling in this case. We show how these mode intensities vary with respect to each other in Fig. 2(b). We find that the intensities evolve toward a limit cycle attractor.

The effects of the interference term appearing in Eq. (3.2) are most easily determined from a plot of $|\cos[\Delta\theta_{01}(t)]|$ versus the intensity of one of the modes as shown in Fig. 3. We find that $|\cos[\Delta\theta_{01}(t)]|$ varies from

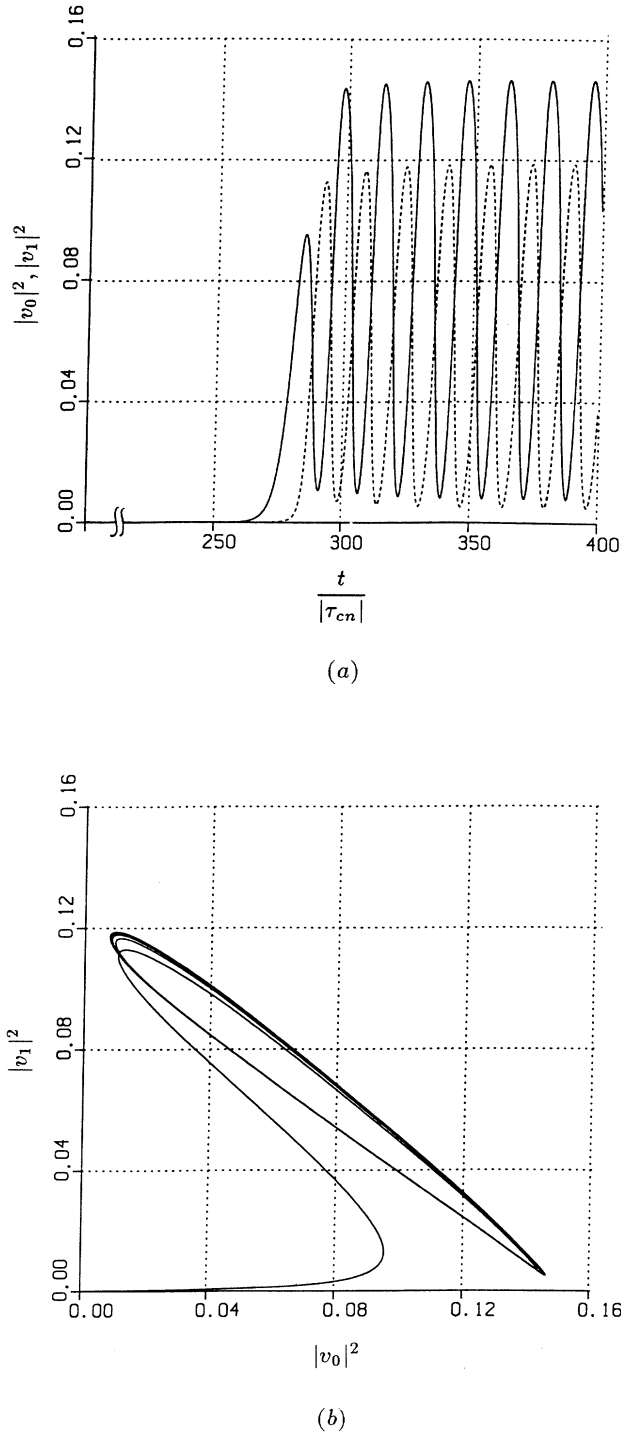


FIG. 2. (a) Oscillations of the intensities of the H_{00} mode $|v_0^2|$ (solid line) and the H_{01} mode $|v_1^2|$ (short-dashed line) as a function of normalized time. (b) Intensity $|v_1^2|$ vs $|v_0^2|$ showing the attracting limit cycle. Parameters values are representative of those for a UPRR containing a KNbO_3 crystal: $a_0 = -1.6 \times 10^9 - i1.6 \times 10^9 \text{ s}^{-1}$, $a_1 = -1.601 \times 10^9 - i1.61 \times 10^9 \text{ s}^{-1}$, $b_0 = b_1 = i9.25 \times 10^{13} \text{ W s}^{-1} \text{ cm}^{-2}$, $c_{01} = i2.313 \times 10^{13} \text{ W s}^{-1} \text{ cm}^{-2}$, $c_{10} = i3.143 \times 10^{13} \text{ W s}^{-1} \text{ cm}^{-2}$, $d_0 = d_1 = 1.0 \times 10^{-5} + i4.0 \times 10^{-5} \text{ cm}^2 \text{ W}^{-1} \text{ s}^{-1}$, $d_{01} = d_{10} = 4d_0$, $f_0 = f_1 = -1.25 + i1.25 \times 10^{-1} \text{ s}^{-1}$, and $f_{01} = f_{10} = f_0/2$.

nearly zero at the minima and maxima of the mode intensity variations to a value near 0.7 in the middle region of the curve. When the modes are at nearly the same intensity, this term is approximately 0.62. The interference term adds the most to the total intensity when the two modes are the same intensity and the least when the modes are at their minima or maxima. This is typical behavior for a dynamical system that oscillates between two complex variables.

The spatiotemporal evolution of the transverse intensity distribution as a function of time is shown in Fig. 4. We have selected a short time segment that includes oscillations from one mode to the other and back again, as seen in Fig. 2. We have found that the two modes mix in a specific manner, as can be observed from the sequence we have shown.

Finally, through numerous numerical simulations we have observed the following trends from our model.

(i) If a_{nr} and a_{ni} are substantially different for two modes, the modes no longer exchange large amounts of energy and their intensities vary only slightly. In some cases, we have also found a reduction of the contribution from the interference term in Eq. (3.2) when $a_{nr} > a_{mr}$ and $a_{ni} = a_{mi}$. This may correspond to the experimental result of Hennequin *et al.* [8], who found that the interference term did not provide a significant contribution to the total resonator intensity for certain two-mode combinations that have a significant difference in their losses.

(ii) As d_{mni} becomes much greater than d_{ni} the mode alternation proceeds more rapidly. This is due to the increase in the mode coupling, which allows more rapid energy transfer. For $|d_{mn}|$ approximately equal to or greater than $|d_n|$ and when $|\tau_{cmn}|$ is slightly smaller than $|\tau_{cn}|$, two-mode coupling will occur. Consequently, very large applied or photovoltaic fields are not necessary to achieve mode coupling.

(iii) If $|\tau_{cmn}|$ becomes much smaller than $|\tau_{cn}|$ intensity spiking occurs. In this case both modes simultaneously become large, decay, and then grow again in a repeated process.

B. Three modes

In order to determine mode coupling effects on a large number of modes, we have examined the three-mode dynamics as a special case. In this case, we consider a UPRR that is limited to having only the H_{00} , H_{10} , and H_{20} Hermite-Gaussian modes in oscillation. An example of the time dynamics possible with three-mode coupling, and multiple-mode oscillations in general, is shown in Figs. 5(a) and 5(b).

The spatial intensity distribution in the three-mode case at two times is shown in Fig. 6. We have found that the intensity variations in these distributions are not as distinct as in the two-mode case. This is due to the simultaneous overlap of the multiple modes, which tends to obscure some of the interference effects. It also leads to the central beam location having a higher average intensity than the off-axis regions, since two of the modes have large central beam amplitudes.

In other numerical simulations, we have found that

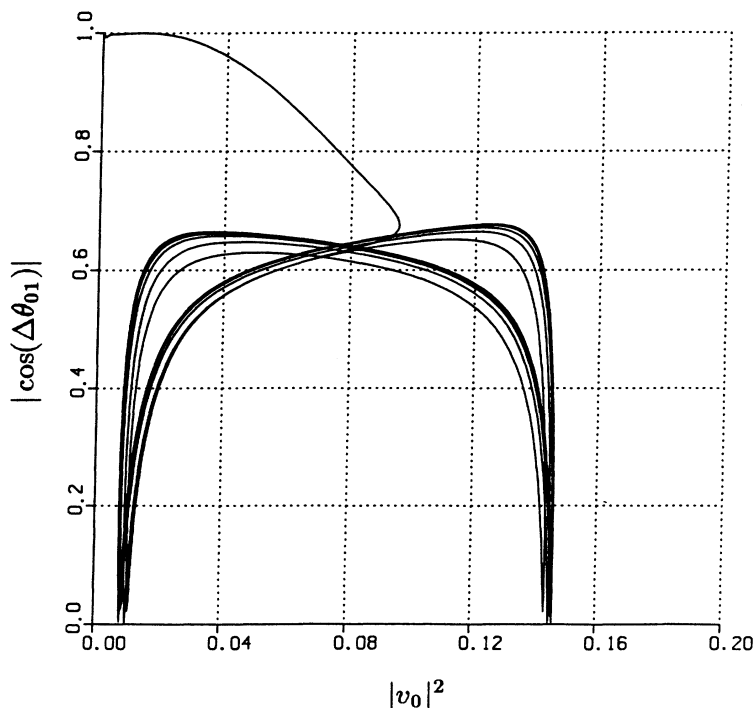


FIG. 3. The magnitude of the intermodal phase difference $|\cos\Delta\theta_{01}(t)|$ vs the intensity of the H_{00} mode, $|v_0|^2$, for the same parameter values used to obtain Figs. 2(a) and 2(b). A similar plot results if $|v_0|^2$ is replaced by $|v_1|^2$ for the abscissa.

three modes can coexist even if they have a fairly large difference in their loss coefficients. Simulations run without intermodal gratings indicate that this will not occur. Consequently, in our model, intermodal gratings permit the simultaneous multiple-transverse-mode oscillations in UPRRs.

IV. EXPERIMENTAL RESULTS

Multiple-mode UPRR experiments were performed using the setup shown in Fig. 1. An Fe:KNbO₃ crystal, which is photovoltaic, was used as the gain medium. In conjunction with our theoretical model, we attribute the occurrence of the strong mode coupling to the photovoltaic electric field.

The crystal was optically pumped using an expanded

and nearly uniform beam from an argon ion laser operating at 514.5 nm. The pump power density was approximately 50 mW cm^{-2} at the crystal surface. The pump and resonator beams made an angle of 30° . The cavity was 150 cm long and contained a lens with a focal length of 100 cm to stabilize the optical oscillations. To limit the resonator oscillations to only a few modes, we placed an adjustable rectangular aperture inside the cavity. Spatiotemporal data were obtained by placing a charge coupled device (CCD) array camera at the output and recording the results on a videotape.

The resonator losses, which were measured to be approximately 40%, were dominated by the reflection and absorption losses at the photorefractive crystal. The partially transmitting mirror reduced the resonator intensity by less than 5%. Consequently, the mean field approxi-

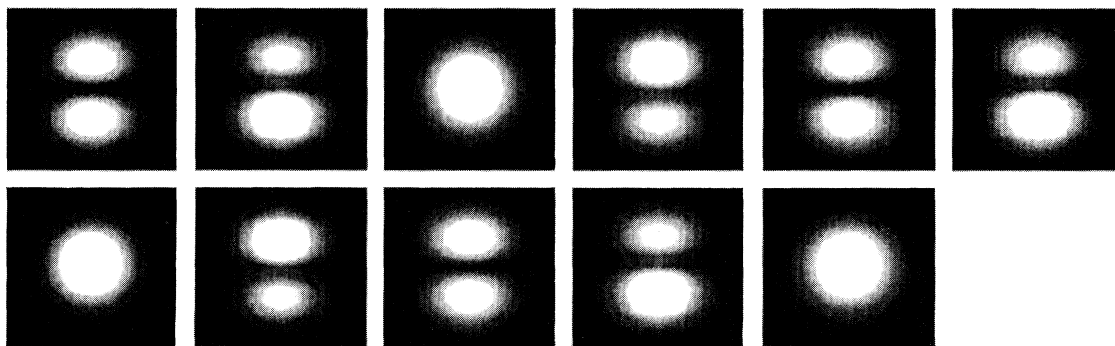


FIG. 4. Theoretical results showing the spatiotemporal evolution of the intensities of the two lowest-order resonator modes for the same parameters used to obtain Figs. 2(a), 2(b), and 3. Time increases from the upper left figure, across the top row, to lower left and across the bottom row. (Compare with the experimental results of Fig. 7).

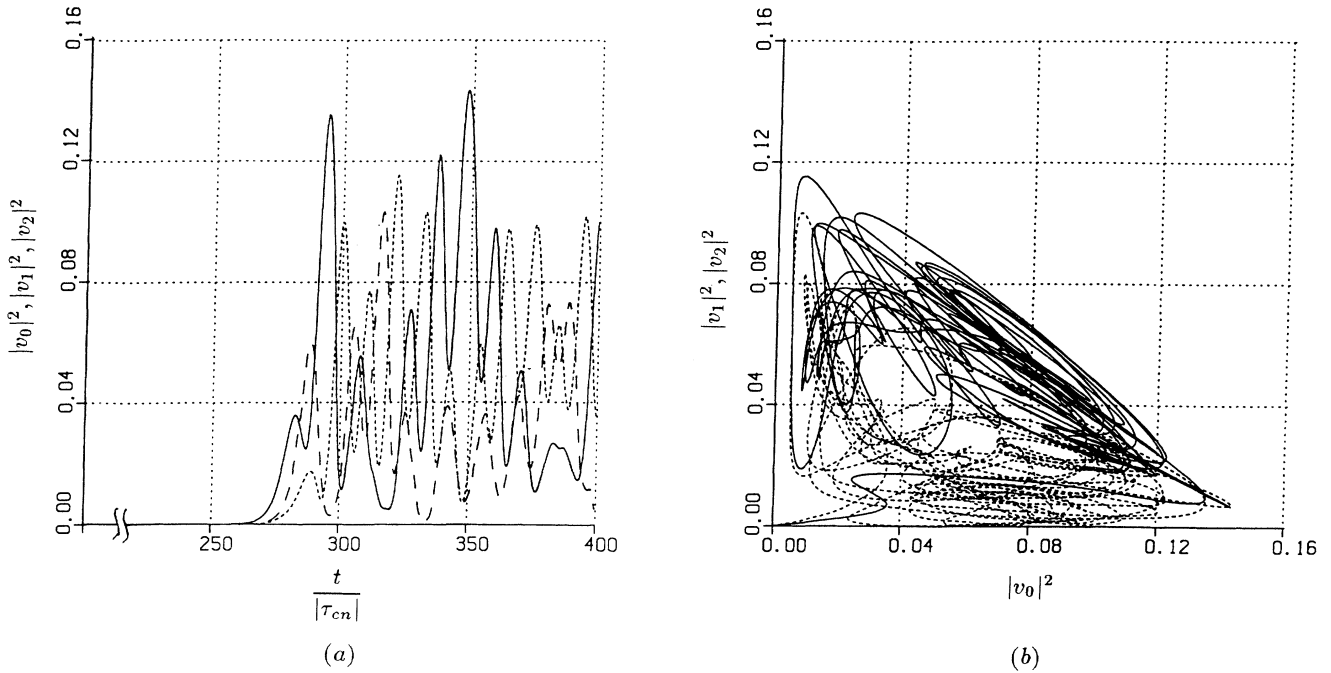


FIG. 5. Mode dynamics when the UPRR is limited to three-mode oscillations. (a) Intensities of the H_{00} mode $|v_0|^2$ (solid line), H_{10} mode $|v_1|^2$ (short-dashed line), and H_{20} mode $|v_2|^2$ (long-dashed line) as a function of normalized time. (b) Intensities $|v_1|^2$ (solid line) and $|v_2|^2$ (short-dashed line) vs $|v_0|^2$. Parameter values are similar to those used to obtain the results shown in Fig. 2: $a_0 = a_1 = a_2 = -1.6 \times 10^9 - i1.6 \times 10^9 \text{ s}^{-1}$, $b_0 = b_1 = b_2 = i9.25 \times 10^{13} \text{ W s}^{-1} \text{ cm}^{-2}$, $c_{01} = i2.313 \times 10^{13} \text{ W s}^{-1} \text{ cm}^{-2}$, $c_{10} = i3.143 \times 10^{13} \text{ W s}^{-1} \text{ cm}^{-2}$, $c_{02} = i1.734 \times 10^{13} \text{ W s}^{-1} \text{ cm}^{-2}$, $c_{12} = i2.750 \times 10^{13} \text{ W s}^{-1} \text{ cm}^{-2}$, $c_{20} = i2.641 \times 10^{13} \text{ W s}^{-1} \text{ cm}^{-2}$, $c_{21} = i3.081 \times 10^{13} \text{ W s}^{-1} \text{ cm}^{-2}$, $d_0 = d_1 = d_2 = 1.0 \times 10^{-5} + i4.0 \times 10^{-5} \text{ cm}^2 \text{ W}^{-1} \text{ s}^{-1}$, $d_{01} = d_{10} = d_{12} = d_{21} = d_{02} = d_{20} = 4d_0$, $f_0 = f_1 = f_2 = -1.25 + i1.25 \times 10^{-1} \text{ s}^{-1}$, and $f_{01} = f_{10} = f_{12} = f_{21} = f_{20} = f_{02} = f_0/2$.

mation that was used in Sec. II, which requires small cavity losses, is probably near the limits of its applicability. Note that, as in other experiments of this type [8], the stability of the resonator oscillations depends on external factors such as table vibrations, air flow, heating or cooling of the crystal, and pump laser variations. As a result, we expect the resonator to be stable for only short periods of time, roughly on the order of one minute.

A. Two modes

In the two-modes case, we adjusted the size of the aperture until only two of the lowest-order modes could oscillate, in which case the aperture size was about 1.0

mm by 1.2 mm. The evolution of the spatially varying resonator beam intensity as a function of time is shown in Fig. 7. This series of snapshots clearly shows the mode mixing. One mode initially dominates. It slowly decreases in amplitude until the second mode dominates. The situation then reverses with the second mode decreasing in amplitude until the first mode dominates. This process repeats itself in a periodic manner, with the two modes mixing in the manner shown. These results are in generally good agreement with the theoretical results of Fig. 4. Similar experimental results showing periodic two-mode oscillations, while using an applied electric field on a $\text{Bi}_{12}\text{GeO}_{20}$ crystal, have recently been obtained by Hennequin *et al.* [8].

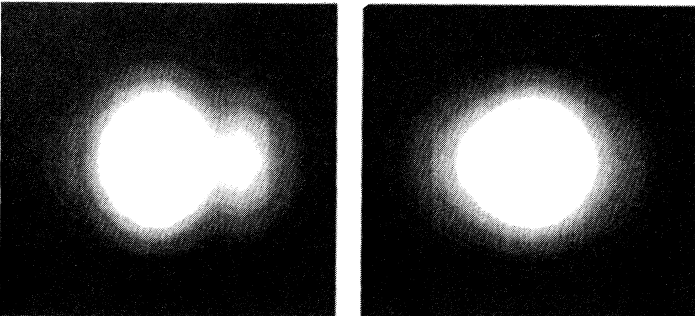


FIG. 6. Theoretical results showing the spatiotemporal evolution of the intensities of the three lowest-order resonator modes for the same parameters used to obtain Figs. 5(a) and 5(b). The excerpts were taken at two different values of $t/|\tau_{cn}|$: left excerpt at 300 and right excerpt at 400. (Compare with the experimental results of Fig. 8.)

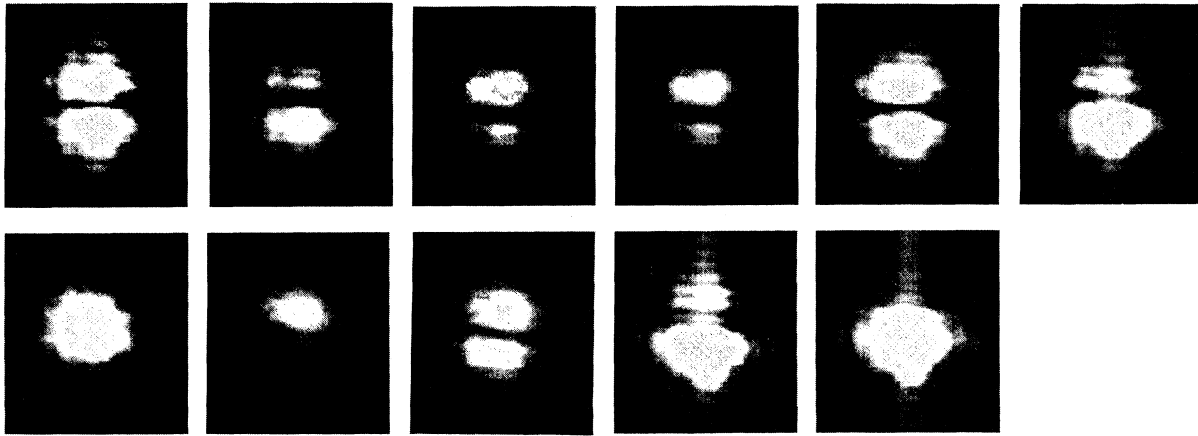


FIG. 7. Experimental results showing the spatiotemporal two-mode interaction. Time increases from the upper left figure, across the top row, to lower left, and across the bottom row. The snapshots are sequentially separated in time by approximately 1 s.

B. Three modes

In the three-mode case, we adjusted the size of the aperture until three of the lowest-order modes could oscillate, in which case the aperture size was about 1.4 mm by 1.0 mm. A very weakly oscillating fourth mode was also observed but we expect the effects of this mode to be negligible because of its small magnitude. However, because the fourth mode was weakly oscillating, it is reasonable to assume that the losses of the three stronger modes were comparable.

Snapshots of the spatial intensity distributions at two times are shown in Fig. 8. These results show good correspondence with those from the theoretical investigation (Fig. 6). We also observed the temporal variations in the spatial intensity distribution due to changes in the various mode amplitudes. This behavior was in general agreement with the theoretical description of Sec. III.

V. DISCUSSION

It is clear that the modal decomposition significantly simplifies the description of the resonator spatiotemporal dynamics when there are only a few modes. However, as the number of modes increases, so does the number of parameters that need to be specified and so do the cumula-

tive errors in any calculations based on uncertain parameter values. Consequently, a partial-differential-equation description of the resonator field, like that given by the photorefractive ring resonator complex Ginzburg-Landau equation [10], may be a more efficient approach to the analysis of the spatiotemporal dynamics when many modes can oscillate. The trade-off, of course, is the increase in computational complexity in the evaluation of such an equation.

In our analysis, we have assumed that longitudinal variations of the slowly varying complex variables were negligible and that the pump remained undepleted. Modifying the present theory to include both longitudinal resonator and pump beam variations would lead to improvements in the accuracy of the results and extend the domain of parameters over which the theory is valid. Taking a more complete account of the effects of the transverse variations would also improve the accuracy of the theoretical description. Such analyses are expected to be straightforward but would require a more complicated description of the resonator. However, these modifications would be a significant step toward the development of a complete description of photorefractive ring resonator phenomena.

In conclusion, we have derived a set of equations that

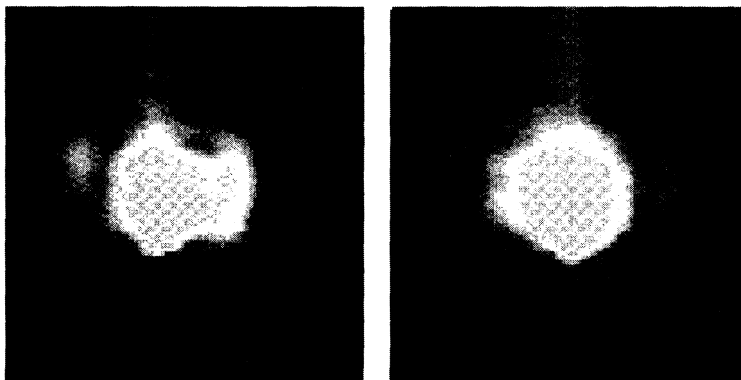


FIG. 8. Experimental results for the spatiotemporal evolution of the resonator modes with three-mode coupling at two times. The left snapshot is separated in time from the right snapshot by 36 s.

describes coupled-mode interactions in unidirectional photorefractive ring resonators when intermodal gratings are formed. We have also performed experiments to observe two- and three-mode coupling effects. Despite many simplifying approximations, we obtained good qualitative agreement between the theoretical analysis

and the experimental data. Hence our results indicate that modal interactions can have a significant effect on the dynamic evolution of the mode fields within photorefractive ring resonators, particularly when there are externally applied or photovoltaic induced electric fields across the crystal.

-
- [1] E. J. Bochove, *Opt. Lett.* **11**, 727 (1986).
 - [2] D. Z. Anderson and R. Saxena, *J. Opt. Soc. Am. B* **4**, 164 (1987).
 - [3] S. R. Liu and G. Indebetouw, *J. Opt. Soc. Am. B* **9**, 1507 (1992).
 - [4] S. R. Liu and G. Indebetouw, *Opt. Commun.* **101**, 442 (1993).
 - [5] F. T. Arecchi, G. Giacomelli, P. L. Ramazza, and S. Residori, *Phys. Rev. Lett.* **65**, 2531 (1990).
 - [6] F. T. Arecchi, G. Giacomelli, P. L. Ramazza, and S. Residori, *Phys. Rev. Lett.* **67**, 3749 (1991).
 - [7] F. T. Arecchi, S. Boccaletti, G. B. Mindlin, and C. Perez Garcia, *Phys. Rev. Lett.* **69**, 3723 (1992).
 - [8] D. Hennequin, L. Dambly, D. Dangoisse, and P. Glorieux, *J. Opt. Soc. Am. B* **11**, 676 (1994).
 - [9] G. D'Alessandro, *Phys. Rev. A* **46**, 2791 (1992).
 - [10] B. M. Jost and B. E. A. Saleh (unpublished).
 - [11] Z. Chen and N. B. Abraham, *Appl. Phys. B* (to be published).
 - [12] E. J. D'Angelo, E. Izaguirre, G. B. Mindlin, G. Huyet, L. Gil, and J. R. Tredicce, *Phys. Rev. Lett.* **68**, 3702 (1992).
 - [13] D. Dangoisse, D. Hennequin, C. Lepers, E. Louvergneaux, and P. Glorieux, *Phys. Rev. A* **46**, 5955 (1992).
 - [14] Q. Feng, J. V. Moloney, and A. C. Newell, *Phys. Rev. Lett.* **71**, 1705 (1993).
 - [15] M. Brambilla, M. Cattaneo, L. A. Lugiato, R. Pirovano, F. Prati, A. J. Kent, G.-L. Oppo, A. B. Coates, C. O. Weiss, C. Green, E. J. D'Angelo, and J. R. Tredicce, *Phys. Rev. A* **49**, 1427 (1994), and references therein.
 - [16] A. B. Coates, C. O. Weiss, C. Green, E. J. D'Angelo, J. R. Tredicce, M. Brambilla, M. Cattaneo, L. A. Lugiato, R. Pirovano, F. Prati, A. J. Kent, and G.-L. Oppo, *Phys. Rev. A* **49**, 1452 (1994), and references therein.
 - [17] B. M. Jost and B. E. A. Saleh, *J. Opt. Soc. Am. B* **11**, 1864 (1994).
 - [18] G. Pauliat, M. Ingold, and P. Gunter, *IEEE J. Quantum Electron.* **25**, 201 (1989).
 - [19] N. V. Kukhtarev, V. B. Markov, and S. G. Odulov, *Zh. Tekh. Fiz.* **50**, 1905 (1980) [*Sov. Phys. Tech. Phys.* **25**, 1109 (1980)].
 - [20] R. De Vre, M. Jeganathan, J. P. Wilde, and L. Hesselink, *Opt. Lett.* **19**, 910 (1994).
 - [21] J. P. Huignard and P. Gunter, in *Photorefractive Materials and Their Applications II*, edited by P. Gunter and J. P. Huignard (Springer-Verlag, Berlin, 1988), Chap. 6, p. 219.
 - [22] A. Yariv and S. K. Kwong, *Opt. Lett.* **10**, 454 (1985).
 - [23] G. Danglemayr and E. Knobloch, *Nonlinearity* **4**, 399 (1991).
 - [24] Mitchell and Gauthier Associates (MGA) Inc., Concord, MA 01742.

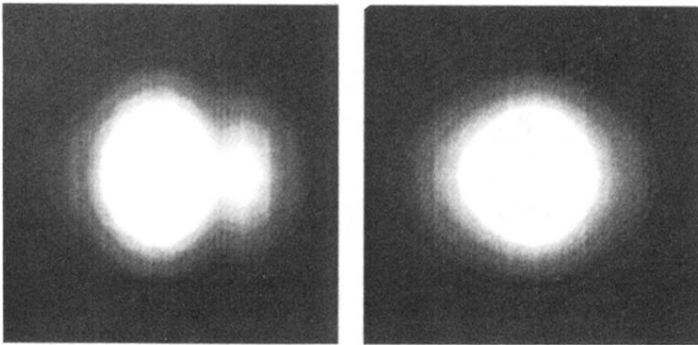


FIG. 6. Theoretical results showing the spatio-temporal evolution of the intensities of the three lowest-order resonator modes for the same parameters used to obtain Figs. 5(a) and 5(b). The excerpts were taken at two different values of $t/|\tau_{cn}|$: left excerpt at 300 and right excerpt at 400. (Compare with the experimental results of Fig. 8.)

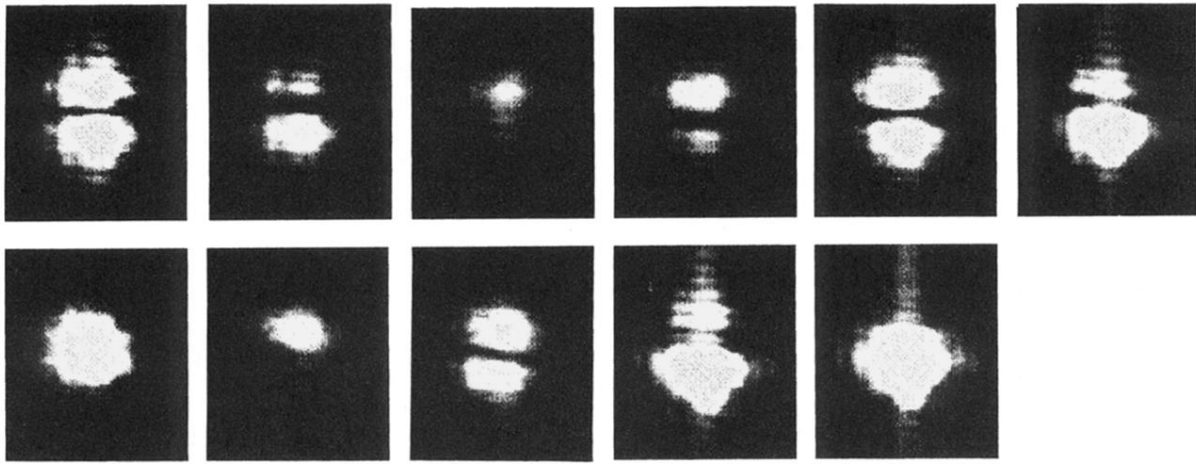


FIG. 7. Experimental results showing the spatiotemporal two-mode interaction. Time increases from the upper left figure, across the top row, to lower left, and across the bottom row. The snapshots are sequentially separated in time by approximately 1 s.

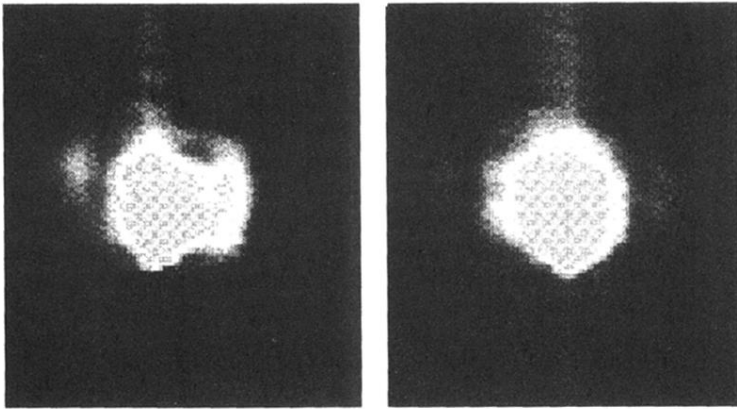


FIG. 8. Experimental results for the spatiotemporal evolution of the resonator modes with three-mode coupling at two times. The left snapshot is separated in time from the right snapshot by 36 s.